DIPOLE FORCE TRAP FOR TRANSPORTING NEUTRAL ATOMS

Chuah Boon Leng

An academic exercise presented in partial fulfilment for the degree of Bachelor of Science with Honours in Physics.

Supervisor: Asst. Prof. BARRETT, Murray Douglas

Department of Physics

National University of Singapore

2007/2008

Acknowledgements

This project would not have been possible without the help and support of the people in Cold Atoms Group.

Thanks to my supervisor Murray, for his instruction and guide along the way, and for his patience and kindness in answering the questions I have.

Special thanks to Kyle, for helping me along the experiment, and for his encouragement and insightful discussion whenever I encountered difficulties in the project.

And not forgetting all the people working in the laboratory, I thank them for always kindly supporting me whenever I need help and assistance. It has been a pleasure working with them.

Boon Leng

4 April 2008

Abstract

The transport of neutral Rubidium 87 atoms was successfully done by moving a focused-beam trap. The atoms were first laser-cooled to the scale of 10μK range and loaded into a dipole force trap. Then the trap was transported up to 40cm, back and forth between the MOT and the destination chamber. The transport was repeated for different time scales, and the relation between the loss ratio and the transport duration was studied. At the time scale of 0.7 second, as much as 80% of atoms stayed in the trap after being transported for 40cm.

Contents

Chapter 1

Introduction

The aim of my project is to transport neutral atoms from one place to another in a UHV (Ultra-High Vacuum) system using dipole force trap. The idea is to bring laser-cooled atoms to a place with better vacuum condition as well as optical access. A typical experimental setup of MOT (Magneto-Optical Trap), as shown in Fig.(1.1), may use up the accessible space around the vacuum chamber. As one can sees from the picture, optics and diagnostic tools for laser cooling such as camera and system of lenses occupy huge amount of space. Transporting the atoms from one chamber to another allows us to have better optical access to the trap, for instance without the space constraint due to MOT setup, the camera can be placed closer to the chamber and the resolution of the trap image would be higher.

The pressure of the chamber for laser cooling is usually high due to the atom source that releases free atoms into the chamber during the cooling

process. Having high pressure in a chamber would reduce the life time of a trap. The reason is that the life time of a trap depends on its collision rate with the background gas and the collision rate increases as pressure increases. A solution to this problem is to have a setup of two connected chambers with significant pressure differential and move the trap to the chamber with lower pressure after the trap has loaded with laser-cooled atoms. This can significantly increase the life time of the trap and allow further cooling processes to take place such as evaporative cooling, provided that the loss in the number of atoms during the transport is negligible.

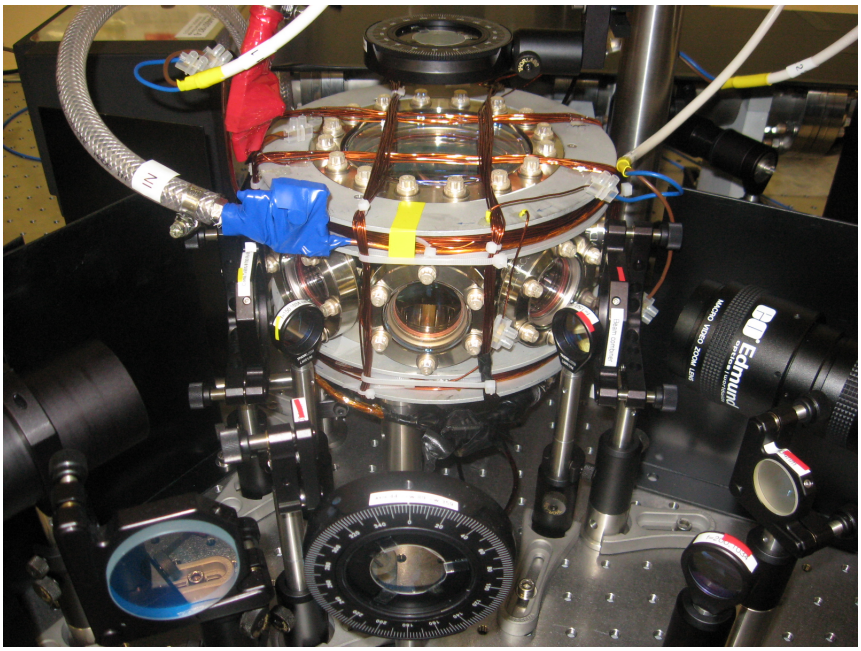

Figure 1.1: **A Typical Setup of MOT.** The accessible room around the chamber has mostly taken up by lenses and diagnostic tool for MOT. This may limit the resolution of the imaging system and further advancement on this chamber.

There are three ways to transport neutral atoms, namely moving standing wave, magnetic transport, and moving dipole force trap. Moving standing wave is achieved using a pair of counter propagating light that points into each other. Light beams with equal frequency form standing wave and neutral atoms stay at the antinodes which have higher intensity. The trapping mechanism is the same as dipole force trap and will be discussed in subsequent chapters. Modulating the frequency of either beam causes the standing wave to propagate in one direction and hence move the atoms from one place to another. However, the transport can only be done for short distances (a few cm) due to the fact that the beam must be tightly focused in order to trap atoms, and as the atoms are transported away from the trap focus, the population fades. Magnetic transport can be done in two ways, either to transport the entire trap mechanically or construct a system of coils and move the magnetic potential by varying the current applied to each coil [1]. However, typical magnetic trap occupies huge amount of space and it may not be as convenient as constructing a dipole force trap. Moving laser-cooled atoms using light trap has already been achieved in free space [2–5] and also within optical fibres [6, 7]. However, only one group in MIT has transported the trap using exactly the same approach as my project, which is moving a dipole force trap by transporting a lens mounted on a motorized translation stage [2].

Dipole force traps have typical potential depths in milli-Kelvin range. In order to load the trap, neutral atoms have to be laser-cooled using MOT down to $\approx 10\mu$K. To get a trap with reasonable life time, Ultra-high vacuum condition is necessary. After the atoms have been cooled and loaded into the

trap, we need a mechanical system that can drive the trap from one place to another. In my project, a motorized translations stage was installed for this purpose. To minimize the loss of atoms during the transport, the mechanical drive must be programmed to move with smooth acceleration. Otherwise the atoms may slosh within the trap and be heated in the process. The transportation is accomplished once the trap arrives to the destination with tolerable loss in number of atoms.

The outline of my thesis is as following: Chapter 2 covers the basic physics of my project, which includes laser cooling and dipole force trap. In Chapter 3, the experimental setup such as vacuum system and optics construction will be presented in details. In subsequent chapters, the results and data of the experiment will be analyzed and discussed. Final chapter emphasizes on the concluding remarks as well as future development and application of the setup.

Chapter 2

Laser Cooling and Trapping

There are essentially three components in light interaction with atoms, namely absorption, spontaneous emission, and stimulated emission. Each of these interactions take part in the following mechanisms that eventually lead to cooling and trapping effects.

2.1 Laser Cooling

Laser cooling is a technique making use of Doppler effect in cooling atoms to the range of $10^2\,\mu K$. The basic physics of this technique is to introduce a velocity dependent force $\vec{F} = -\alpha\vec{v}$ on moving atoms and reduce the kinetic energy of the atoms through light scattering [8, 9]. First, let us start by looking at the interaction between atoms and monochromatic laser beam with frequency ω and intensity I. Interacting with the laser beam, atoms experience scattering. Scattering is a complete circle of light absorption and

spontaneous emission. Atoms absorb photons in one particular direction and emit them randomly in all direction. Overtime, the momentum delivered by the spontaneous emitted photons averages to zero. Hence the time-averaged force only depends on the rate at which the absorbed photons transfer momentum to the atom

$$F = (\text{photon momentum}) \times (\text{scattering rate})\,. \tag{2.1}$$

The scattering rate is [12]

$$R = \frac{\gamma}{2}\frac{I/I_{sat}}{1 + I/I_{sat} + (2\Delta/\gamma)^2} \tag{2.2}$$

where I_{sat} and γ are respectively the saturation intensity and the natural linewidth of the transition, and Δ is the detuning in frequency that could possibly be caused by two factors, either the light is of off-resonance frequency or Doppler-shift in light frequency due to relative motion between the atom and the light field. A photon has momentum $\hbar k$, so the scattering force can be written as

$$F = \hbar k\frac{\gamma}{2}\frac{I/I_{sat}}{1 + I/I_{sat} + (2\Delta/\gamma)^2}\,. \tag{2.3}$$

2.1.1 Optical Molasses

Having shown the interaction between a laser beam and an atom, and the way photons transfer momentum to atoms, we now look at laser cooling in three dimensional space or optical molasses. Optical molasses is a

technique that reduces the velocity of an atom regardless of its propagating direction. There are six laser beams that propagate in $\pm x$, $\pm y$, $\pm z$-directions and crossing one another at the same position. The laser frequency is detuned a few natural linewidths below the resonance frequency. Since the intensity of a pair of counter propagating beams are more or less the same, the forces exerted by the beams balance each other for a stationary atom. However, moving atoms always experience repulsive forces due to Doppler effect. The reason is that if an atom is moving towards the laser, then the laser frequency as seen by the atom is Doppler shifted closer to its transition frequency. Hence the scattering rate increases and the atom undergoes deceleration. In result, an atom moving within the overlapping region of the six pair wise counter propagating laser beams experiences a force which is always against its direction of motion. For a quantitative description, let us only look at one dimension. The absorption rate of an atom with $kv_z > 0$ is denoted by $R^+(v_z)$ and for $kv_z < 0$ by R^-. Then the net recoil force is

$$F_z \;=\; \Big(R^+(v_z) \;-\; R^-(v_z)\Big)\,\hbar k\,. \tag{2.4}$$

Modifying eq.(2.3) a bit to explicitly express both the detuning in laser and the velocity of the atom, we have

$$R^{\pm}(v_z) \;=\; \frac{\gamma}{2}\frac{I/I_{sat}}{1 + I/I_{sat} + (2(\frac{\omega_L - \omega_0 \mp k v_z}{\gamma/2})^2}\,, \tag{2.5}$$

where ω_L is the angular frequency of the laser. Eq.(2.4) can be approximated to the following form by neglecting the terms of order $(kv/\gamma)^4$ and higher,

$$F_z \;=\; \frac{8s\delta\hbar k^2}{\gamma\big(1+s+(2\delta/\gamma)^2\big)^2}\, v_z\,, \tag{2.6}$$

where $s = I/I_{sat}$ and $\delta = \omega_L - \omega_0$. Rewriting the force equation in differential form, we have

$$m\frac{dv_z}{dt} \;=\; -a\, v_z\,, \text{ with } \; a \;=\; \frac{8s\delta\hbar k^2}{\gamma\big(1+s+(2\delta/\gamma)^2\big)^2}\,. \tag{2.7}$$

Solving the differential equation, we obtain time-dependent velocity

$$v_z(t) \;=\; v_{z0}\, e^{-(a/m)t}\,. \tag{2.8}$$

Eq.(2.8) shows that the velocity of the atom decreases exponentially with the decay time $T_D = \frac{m}{a}$. This equation also implies that once the atom is in the overlap region of six pair wise laser beams, its velocity could be reduced drastically if T_D is small. For typical setup, T_D is usually on a millisecond scale.

2.1.2 The Doppler Cooling Limit

Using molasses technique, the velocity of the trapped atoms can be reduced to almost zero. At this very cold state, the atoms still experience random kicks from spontaneously emitted photons and absorbed photons. Although the forces exerted by these kicks would eventually average to zero, the random walk of the atom during the interval of the kicks poses a limit

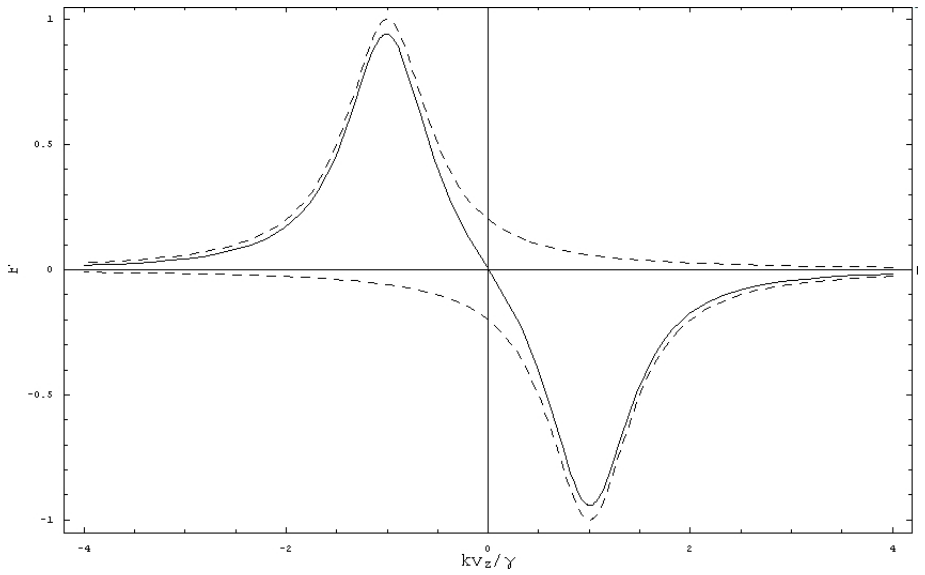

Figure 2.1: **Force as the function of the velocity of atoms in optical molasses for red detuning $\delta = -\mathbf{1}\gamma$.** The dotted curves are the absorption profiles of the atoms moving with $v_z = \pm\gamma/k$ for a single laser beam pointing into z-direction. The force F axis is expressed in the scale of $1/R_0\hbar k$.

to the lowest temperature that optical molasses can achieve. The Doppler cooling limit is given by [10]

$$k_B T_D = \frac{\hbar\gamma}{2}\,, \tag{2.9}$$

$$\text{or} \quad = \frac{\hbar}{2\tau}\,. \tag{2.10}$$

For D_2 transition of Rubidium 87 with lifetime $\tau = 26.24$ns, the Doppler cooling limit is 146μK.

2.1.3 MOT - Magneto-Optical Trap

Optical molasses is an efficient way to cool neutral atoms. However, the density of the trap is too low to load a dipole force trap which has the trap size that typically in micron range. When the technique was first realized in 1985, the density of the trapped atoms was only around 10^6cm^{-3} [8]. To increase the density of the trap, one solution is to exert position dependent force on the atoms that have been trapped by optical molasses such that the atoms gather themselves at certain position after being laser-cooled. A technique that serves this purpose, incorporating both optical molasses and magnetic quadrupole field which is now known as MOT (Magneto-Optical Trap), was realized in 1987 and the trap density was exceeding 10^{11}cm^{-3} [11].

The optical setup for MOT is almost the same as optical molasses, however the mode of the light field is chosen to be circular polarization (σ^+, σ^-) instead of linear polarization (π^0). The reason for that will be further explained in the following part of this section. The magnetic quadrupole field is produced by a pair of coils with anti-Helmholtz configuration. The configuration is such that the net magnetic field is zero at the origin with constant magnetic field gradient along the coaxial axis of the coils. To illustrate how the trap works, let us consider atomic transition with a simple scheme of $J_g = 0 \rightarrow J_e = 1$ that has three Zeeman components in excited states, each excited by one of the three polarizations (σ^+, σ^-, π^0) as shown in Fig.(2.2). The magnetic field around the origin shifts the Zeeman energy level of the atoms as illustrated in Fig.(2.3). Referring to the same figure, we see that the effect is such that $M_L = +1$ is shifted away from the laser frequency at $+x$

side to the origin while $M_L = -1$ exhibits the opposite behaviour. Consider an atom that stays at certain $+x$ position near the origin, the scattering rate from σ^- would be higher than σ^+ as the energy level of $M_L = -1$ is closer to the laser frequency. Thus the resultant radiation pressure would be pointing towards $-x$ direction, and consequently the atom moves towards the origin. Similarly, the atoms that stay at the $-x$ side would also experience a net force that pushing them towards the origin. Hence the laser-cooled atoms around the origin would eventually gather themselves and form an atoms cloud with the density that approximately 10^5 higher than the trap by optical molasses alone. For quantitative description, the net force due to the scattering from both counter propagating beams is [10]

$$\begin{aligned} F &= F_{\sigma^+}(\omega - kv - (\omega_0 + \beta x)) - F_{\sigma^-}(\omega + kv - (\omega_0 - \beta x)) \quad (2.11) \\ &\approx -2\frac{\partial F}{\partial \omega} kv + 2\frac{\partial F}{\partial \omega_0}\beta x \,. \quad (2.12) \end{aligned}$$

Where $\omega_0 + \beta x$ is the resonant absorption frequency for σ^+ transition at position x and $\omega_0 - \beta x$ is that for σ^-. The Zeeman shift at position x is given by

$$\beta x = \frac{g_J \mu_B}{\hbar}\frac{dB}{dx}x \,. \quad (2.13)$$

Since the force depends on frequency detuning $\Delta = \omega - \omega_0$,

$$\frac{\partial F}{\partial \omega} = -\frac{\partial F}{\partial \omega_0}. \quad (2.14)$$

Hence the net force can be written as

$$F = -2\frac{\partial F}{\partial \omega}(kv + \beta x) \tag{2.15}$$

$$= -\alpha v - \frac{\alpha\beta}{k}x\,, \tag{2.16}$$

where $\alpha = 2k\frac{\partial F}{\partial \omega}$. From eq.(2.16), we see that the imbalance in radiation force due to Zeeman effect leads to a restoring force with spring constant $\alpha\beta/k$. Solving eq.(2.16), we have the damping rate given by α/m and the oscillation frequency $\sqrt{\alpha\beta/km}$, where m is the mass of an atom. For temperature in Doppler cooling range, the size of a typical atoms cloud should be of the order of a few tenths of a mm [12].

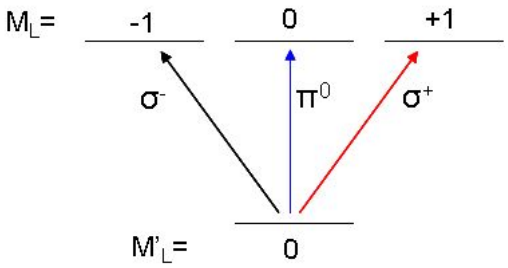

Figure 2.2: **Atomic Transition of $\mathbf{J_g = 0 \rightarrow J_e = 1}$.** σ^+, σ^-, and π^0 are respectively clockwise, anti-clockwise, and linear polarizations. Each of these polizations only corresponds to one of the transitions at Zeeman energy level.

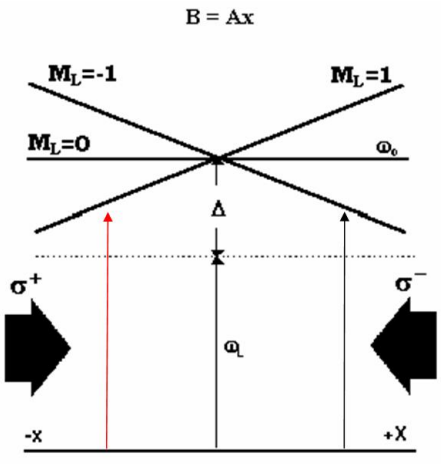

Figure 2.3: **Zeeman Effect - Shifts in Transition Energy Level.** Δ is the detuning of the laser, ω_L is the laser frequency, and ω_0 is the natural frequency of the π transition or the $J_g = 0 \rightarrow J_e = 1$ transition without the magnetic filed. Black and red arrows represent σ^- and σ^+ transitions, respectively.

2.2 Dipole Force Trap

The physical origin of a dipole force trap is the optically induced shift in atomic energy level or ac Stark shift due to the interaction between the light field and atoms. In fact this shift in energy level has the same physical origin as DC stark shift. For inhomogeneous and below resonance light, this interaction creates an attraction that causes the atoms to move towards the high intensity region [13, 14], and this is the basic idea of trapping atoms using red-detuned light. The shift in energy level, as illustrated in Fig.(2.4), leads to the following expressions for both potential energy and scattering rate [15]

$$U_{dip}(\vec{r}) = -\frac{3\pi c^2}{2\omega_0^3}\frac{\Gamma}{\Delta}I(\vec{r}), \tag{2.17}$$

$$\Gamma_{sc}(\vec{r}) = \frac{3\pi c^2}{2\hbar\omega_0^3}\left(\frac{\Gamma}{\Delta}\right)^2 I(\vec{r}). \tag{2.18}$$

Where ω_0 is the resonant angular frequency of the transition, Γ is the damping rate or the spontaneous decay rate of the excited state, Δ is the detuning $\omega - \omega_0$, and $I(\vec{r})$ is the position dependant light intensity. Eq.(2.17) and Eq.(2.18) are both the results from rotating-wave approximation where those counter-rotating terms, with $\omega+\omega_0$ as their denominator, in these expressions have been neglected. According to eq.(2.17), the sign of detuning determines whether the trap attracts or repels atoms. Below an atomic resonance, or "red detuning", the trap potential is negative and hence attracts atoms towards the light field. The minimum of the potential is therefore found at the region with maximum intensity.

An optimum trap should have reasonable potential depth and negligible scattering rate such that the heating due to scattering is insignificant. Dipole force potential and scattering rate are respectively proportional to I/Δ and I/Δ^2. When the detuning is large, the amount of decrease in scattering rate is much significant as compared to potential depth. However, laser with large detuning also reduces the trap depth. To compensate this undesired effect, high power laser is needed. Hence laser with high power and large detuning is typically used for making a dipole force trap.

In my project, a focused-beam trap was used. Focused-beam traps are usually achieved using a convex lens and a collimated beam with the beam waist in millimetre range. The role of the lens is to create a high intensity focus with the beam waist in the range of a few tenths of a micron. The final beam waist w_{02} can be related to the initial beam waist w_{01} through following equation,

$$w_{02} = \frac{\lambda f}{\pi w_{01}}, \tag{2.19}$$

provided that $\pi w_{01}^2/\lambda >> f$ and this is true in most cases. For this trap, the spatial intensity distribution, as shown in Fig.(2.5), of the laser beam with power P is described by

$$I(r,\, z) = \frac{2P}{\pi w^2(z)}\, exp\Big(-2\frac{r^2}{w^2(z)}\Big), \tag{2.20}$$

where

$$w(z) = w_0\sqrt{1+\Big(\frac{z}{z_R}\Big)} \tag{2.21}$$

$$\text{and } z_R = \frac{\pi w_0^2}{\lambda}. \tag{2.22}$$

We can see from eq.(2.20) that the intensity is highest at the focus where $r = 0,\ z = 0$. This creates a trap providing three dimensional confinement. In the region close to the focus, a simple cylindrically symmetric harmonic oscillator can be a good approximation to describe the trap potential,

$$U \approx -U_0\left(1 - 2\left(\frac{r}{w_0}\right)^2 - \left(\frac{z}{z_R}\right)^2\right). \tag{2.23}$$

Referring to eq.(2.23), the oscillation frequencies of a trapped atom with mass m along radial and axial axes are given by $\omega_r = \sqrt{4U_0/mw_0^2}$ and $\omega_z = \sqrt{2U_0/mz_R^2}$, respectively. The oscillation frequency along axial axis is particularly important for calculating the equation of motion of the atom throughout the transport.

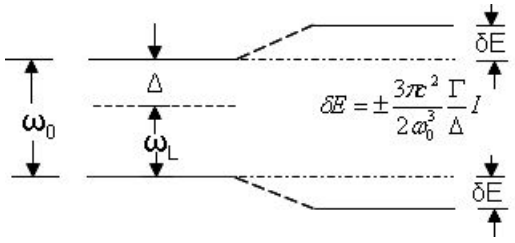

Figure 2.4: **Stark Shift.** ω_L is the light frequency and Δ is the detuning.

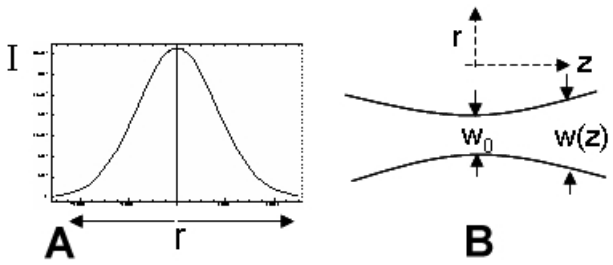

Figure 2.5: **The Intensity Distribution and The Beam waist.A:** The intensity distribution of TEM00 mode laser beams follows Gaussian profile along radial axis. **B:** Typical view of a focused-beam waist.

2.2.1 Sub-Doppler Cooling

To load a dipole force trap efficiently, it is always helpful if the temperature of the atoms can be further reduced. Sub-Doppler cooling is a fruitful technique in achieving this purpose because it manages to bring the temperature down to microKelvin range. There are many kinds of sub-Doppler cooling mechanisms. In my experiment, the resultant field of six pair wise counter propagating beams may lead to the present of more than one kind of sub-Doppler cooling. The details of these cooling processes are beyond the scope of my project. However, in order to briefly introduce this technique, Sisyphus cooling is chosen to be presented in this part. Part of the reason is that the mechanism of Sisyphus cooling is relatively straight forward as compared to the rest of sub-Doppler cooling techniques. In Sysiphus cooling, counter propagating light beams forms standing wave as shown in Fig.(2.6). For any atom in motion, it has to climb up the dipole potential induced by the standing wave of the laser beams. Upon reaching the top of the potential hill, the atom is scattered and optically pumped back into the bottom of the next potential valley. Such a process suggests that the atom will keep on moving until its energy is no longer higher than the peak of the potential hill and remain stuck in the valley. Hence the cooling limit of Sysiphus cooling is set by the potential depth of the standing wave, and is usually a few times the recoil energy [10].

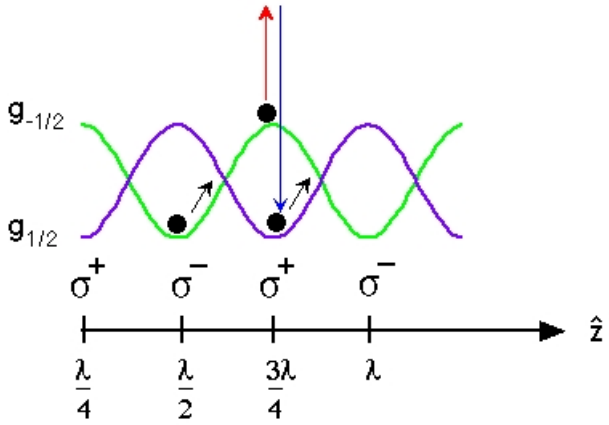

Figure 2.6: **Sysiphus cooling.** The counter propagating light with their polization axes perpendicular to each other results in forming standing wave with different polarization modes at different location. SubDoppler level $g_{-1/2}$ and $g_{1/2}$ show different coupling behaviours with the light modes and give rise to dipole potential with "hill" and "valley".

Chapter 3

Experimental Setup

3.1 Vacuum System

The depth of optical dipole traps is typically less than 1 mK and so collisions with room temperature atoms results in a loss of atoms and so the trap lifetime will be limited by the background pressure. In order to achieve trap lifetimes exceeding 1 s it is necessary to achieve vacuum pressures well below 10^{-7}Pa or 10^{-9}Torr. In this chapter we outline the necessary steps to achieve such low pressures and discuss some of the design considerations for our chamber.

3.1.1 Conductance

The ultimate pressure P in a vacuum system is given simply by

$$P = \frac{Q}{S} \tag{3.1}$$

where Q is the gas load (in Torr L/s) and S is the pumping speed (in L/s). The gas load is essentially the rate at which particles enter the vacuum chamber and the pumping speed is a measure of the ability of the pump to remove them. The objective is then obvious: minimize the stuff entering the chamber and make the pumping speed as large as possible. Increasing the pumping speed is not as trivial as simply buying a really big pump - it does no good to have a pump with a large pumping speed if the chamber is connected to it through a very small tube. To quantify the effects of the tube connecting the pump to the chamber we need to discuss the notion of conductance.

Conductance

Conductance of a section of the vacuum system is defined by the equation

$$C = \frac{Q}{P_2 - P_1}\,, \tag{3.2}$$

where the throughput Q is the amount of gas that passes a cross-section in a known time $Q = d/dt(PV)$ and $P_2 - P_1$ is the pressure differential [16]. The conductance limits the effective pumping speed at a particular point in the chamber according to the equation

$$\frac{1}{S_{\text{eff}}} = \frac{1}{C} + \frac{1}{S} \tag{3.3}$$

From this equation it is easily seen that a low conductance will be the ultimate limit to the pumping speed to the chamber no matter how large the pumping speed of the pump.

Conductance calculations

In typical vacuum conditions the flow of the gas is characterized by molecular flow [16]. In this regime, if two large vessels are connected by an orifice of area A then the gas flow from one vessel to another is given by

$$Q \;=\; \frac{kT}{4}\, vA\,(n_1 \;-\; n_2) \;=\; \frac{v}{4}\, A\,(P_1 \;-\; P_2)\,, \tag{3.4}$$

where $n_{1,2}$ is the density of gaseous molecules, v is the average thermal velocity of the gas, and $P_{1,2}$ is the pressure of each vessel. By definition, the conductance of the orifice is described by

$$C \;=\; \frac{Q}{P_1 \;-\; P_2} \;=\; \frac{v}{4}\, A\,. \tag{3.5}$$

For a pipe with finite length and diameter, the conductance also depends on the transmission probability a that the gas particles entering the pipe will leave at the other end. Thus the equation describing the conductance of a pipe is

$$C \;=\; a\,\frac{v}{4}\, A\,, \tag{3.6}$$

where $a = a(L)$ is given by [17],

$$a(L) = K_1(L) - K_2(L)\,, \tag{3.7}$$

$$K_1(L) = 1 + \frac{L^2}{4} - \frac{L}{4}\sqrt{L^2+4}\,, \tag{3.8}$$

$$K_2(L) = \frac{\sqrt{(8-L^2)\sqrt{L^2+4}+L^3-16}}{72L\sqrt{L^2+4}-288\ln L+\sqrt{L^2+4}+288\ln 2}\,. \tag{3.9}$$

$L = l/r$ is the reduced length where l and r are the pipe length and radius respectively. A remark on eq.(3.6) is that when the pipe has small L, a approximates 1 and hence eq.(3.6) approximates eq.(3.5), as expected.

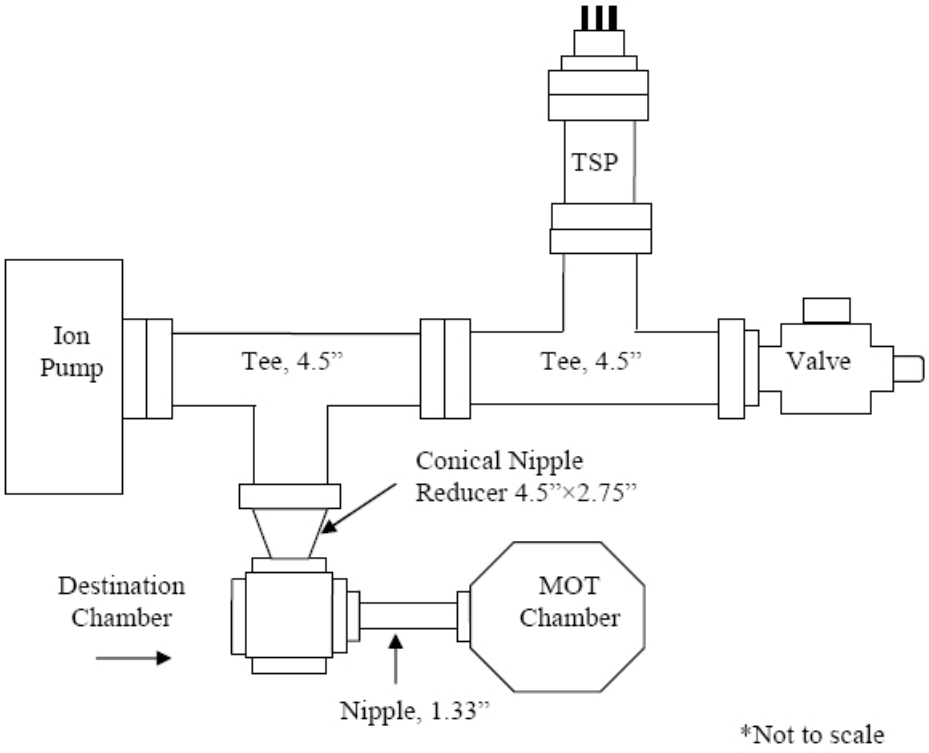

Figure 3.1: **Plan View of The Vacuum System.**

Section	Conductance (L/s)
C_1	47.1
C_2	55.7
C_3	77.0
C_4	5.71

Table 3.1: **Conductance of The Vacuum Components**

The design of my vacuum system is illustrated in Fig.(3.1). In order to know the pressure in the destination chamber and the MOT chamber, the conductance of each part of the system that connects these two chambers to the ion pump must be calculated. Referring to Fig. (3.1), there are four components connecting the MOT chamber to the ion pump, namely 4.5" Tee, nipple reducer, cube or destination chamber, and 1.33" nipple. As a matter of convenience, the conductance of these components are denoted by C_1 to C_4 respectively, according to their arrangement. Details of the calculation of the conductance of each section is given in the appendix and the results given in the table below

Combining conductances

The total can be estimated by [16],

$$\frac{1}{C} = \sum_j \frac{1}{C_j}\,. \tag{3.10}$$

However this equation is only applicable to the case where the individual elements are separated by large volumes, such that the molecules exiting the

prior conductance would have a place to completely randomize their distribution [16]. A more rigorous approach in calculating the total conductance would be to make use of Haefer's method. For the system of $n-$tubes in series connection, the transmission probability $a_{1\to n}$ is described by Haefar's method [16]

$$\frac{1}{A_1}\Big(\frac{1-a_{1\to n}}{a_{1\to n}}\Big) = \sum_1^n \frac{1}{A_j}\Big(\frac{1-a_j}{a_j}\Big) + \sum_1^{n-1}\Big(\frac{1}{A_{j+1}} - \frac{1}{A_j}\Big)\delta_{j,j+1}\,, \quad (3.11)$$

where A_j and a_j are the respective cross-sectional area and transmission probability of the $j-$section of the pipe, $\delta_{j,j+1} = 1$ for $A_{j+1} < A_j$, and $\delta_{j,j+1} = 0$ for $A_{j+1} \geqslant A_j$. The corresponding expression for the conductance is similar to eq.(3.6),

$$C = \big(a_{1\to n}\big)\frac{v}{4}A_1 = \big(a_{n\to 1}\big)\frac{v}{4}A_n\,. \quad (3.12)$$

Using these equations we find the overall transmission probability from the ion pump to the MOT chamber a_{MOT} is given by

$$\begin{aligned}\frac{1}{A_4}\Big(\frac{1-a_{MOT}}{a_{MOT}}\Big) &= \frac{1}{A_1}\Big(\frac{1-a_1/2}{a_1/2}\Big) + \frac{1}{A_2}\Big(\frac{1-a_2}{a_2}\Big) + \frac{1}{A_3}\Big(\frac{1-a_3/2}{a_3/2}\Big)\\ &+ \frac{1}{A_4}\Big(\frac{1-a_4}{a_4}\Big) + \frac{1}{A_4} - \frac{1}{A_3}\,.\end{aligned}$$

We note that some of the transmissions probabilities are divided by two to conservatively account for right-angle bend along the corresponding vessels (see the Kurt Lesker website for a discussion on this point). Rearranging and substituting the required parameters into the equation, we have

$$a_{MOT} = 0.0152\,. \tag{3.13}$$

Substituting $A_4 = \pi\,(1.73\,\mathrm{cm}/2)^2$ and eq.(3.13) into eq.(3.12), we arrive at the effective conductance between ion pump and the MOT chamber

$$C_{MOT} = 5.01\,l/s\,. \tag{3.14}$$

Using similar approach to calculate the overall transmission probability a_{dc} and the effective conductance C_{dc} of the destination chamber, we have

$$a_{dc} = 0.125\,, \tag{3.15}$$

$$\text{and } C_{dc} = 41.3\,l/s\,. \tag{3.16}$$

We note that the total conductances using the simple eq.(A.4) we obtain $C'_{MOT} = 4.40\,l/s$ and $C'_{dc} = 25.5\,l/s$.

3.1.2 Vacuum Condition

With eq.(3.14) and eq.(3.16), the pressure differential between the chambers and the ion pump can be calculated. The relation between pumping speed S, throughput Q, and pressure P is described by eq.(3.1). Assuming that the throughput is the same for different compartments of the system, the following equation can be derived from eq.(3.1), eq.(3.2), and eq.(3.3)

$$P_2 = P_1\left(1 + \frac{S}{C}\right), \tag{3.17}$$

this relates the pressure at any location in the system to the pressure at the ion pump through the pumping speed and the conductance between these locations. For my project, the pumping speed S of the ion pump (Varian Vaclon Plus 55) is 55 l/s and the pressure as measured by the ion pump is $\approx 2.0 \times 10^{-10}$. Substituting these parameters into eq.(3.17) to calculate the pressures of interest, we have

$$P_{MOT} = 2.4 \times 10^{-9} \text{ Torr}, \tag{3.18}$$

$$\text{and } P_{DC} = 4.7 \times 10^{-10} \text{ Torr}, \tag{3.19}$$

where P_{MOT} and P_{DC} are the respective pressures inside the MOT and the destination chamber. The pressure difference between these two chambers will mean that the lifetime of the trap will be longer in the destination chamber as much as twice than that in the MOT chamber, as the pressure inside the destination chamber is about one order of magnitude lower than the pressure inside the MOT chamber. This is actually one of the motivations for doing this project: to have a low pressure in the destination chamber with a higher pressure in the MOT chamber to facilitate making a good MOT.

3.1.3 Outgassing

Outgassing is often attributed to all processes that contribute to the gas load in the vacuum system. In ultra-high vacuum conditions the dominate process is desorption of molecules from the walls of the chamber. To minimize this gas load the entire vacuum system is baked at high temper-

ature (as high as possible) to remove the gas molecules that absorbed on and dissolved in the chamber walls. For my project, the vacuum system was baked at 230°C for a week inside an oven chamber where the temperature was limited by the baking limits of some of the vacuum components (the coated windows). Before the bakeout, the rubidium source was fired at 3A for one hour while the mechanical pump was operating and pumping at the pressure of 10^{-6} Torr. This process heats the Rubidium source and facilitates an initial outgassing and cleaning. The same firing process was also done for the titanium sublimation for the same reason.

The bakeout temperature was monitored by four thermocouples that were installed at different locations about the vacuum system to facilitate the measurement of both temperature possible temperature gradients. The pressure of the vacuum system was monitored using an IMG (Inverter Magneton Gauge) which was connected to the top of the mechanical pump, outside the bakeout chamber.

After a week of bakeout, the oven chamber was dismantled. At this stage, the pressure inside the vacuum chamber was in the range of $10^{-8} \rightarrow 10^{-9}$ Torr. At this time the ion pump was switched on and the TSP (Titanium Sublimation Pump) was fired at current of ≈48 A in accordance with the manufacturers specifications. During this time the pressure spiked as the temperature of the filament rose. After about 30 seconds the pressure suddenly decreased indicating that Titanium was being deposited and the TSP was switched off when the rate of decrease in pressure became

slower. The purpose of the TSP is to facilitate the pumping of hydrogen gas since hydrogen sticks to the layer of Ti deposited on the chamber walls.

After firing the TSP the valve was closed to disengage the tubo-molecular pump. Ultimately the pressure in the chamber was reduced to below 10^{-10} Torr which is the limit of the ion pump reading capability and UHV conditions were thus achieved.

3.2 Laser and MOT setup

Two lasers with different wavelength were used in my project. One was 780nm laser which involved in atoms cooling. The other was 1034nm laser which produced high power beam for creating a dipole force trap. 780nm laser beams were produced using commercial laser diodes. Each laser diode was placed inside a metal box that equipped with temperature controller such that the output wavelength of the laser would not be affected by the fluctuation in temperature. Light spectrum of the diode covers the atomic transitions of interests. However, for the interaction at hyperfine energy level, laser with the right transition frequency as well as well-narrowed spectral distribution is required. The required linewidth of transition spectrum must be in the range of natural linewidth, which is the smallest linewidth that one can get. To achieve that, a setup of saturation spectroscopy is needed. Saturation spectroscopy or Doppler-free spectroscopy allows one to locate the hyperfine transition levels by getting rid of Doppler broadening of the atomic spectra due to the random motion of the atoms or molecules in the gaseous

sample [18]. Apart from Doppler broadening, there are also other potential sources that may broaden the spectral linewidth, such as homogeneous broadening for instance, collision broadening and power broadening [19]. However, these broadening are of our little concern because their effects are insignificant in typical atoms cooling experiments. There were two 780nm laser diode used in my experiment, one was served as master laser, the other as slave laser. The Master laser was locked to an Atomic reference cell via saturated absorption spectroscopy. The laser light was then double passed through an Acousto-optic modulator which allows the frequency of the light to be shifted in a controlled way. However the frequency shift was coupled to an intensity change in the light which is undesirable. Moreover the double pass configuration decreased the available power due to the efficiency of the AOM. To alleviate these effects the Master laser was used to seed a second slave laser by injection locking [20, 21]. In this technique a small amount of the Master laser light was directed into the slave which caused the slave to phase lock with the Master. With this set up the Slave laser can be tuned to any frequency within the Bandwidth of the double pass AOM setup with a constant power output of approximately 100mW. The intensity of the slave was controlled by a second AOM. This AOM was operated at a fixed frequency and changing the RF power to the device changes the power in the deflected beam. Upon passing through the AOM, the laser beam was then split and coupled into three optical fibres. The other ends of these fibres were position according to the configuration for laser cooling around the MOT chamber.

In the cooling process, atoms in $F = 2$ first absorb a photon and ex-

perience a transition $F = 2 \rightarrow F' = 3$ as described in Fig.(3.2). Then the atoms only decay spontaneously into $F = 2$. However, the excitation may also happen for transitions $F = 2 \rightarrow F' = 2$ and $F = 2 \rightarrow F' = 1$ due to the detuning in light frequency. Hence some of the atoms may also decay into $F = 1$. Since the atoms in $F = 1$ will not be excited by the laser, most of the atoms will eventually end up in $F = 1$ and consequently the cooling process will be stopped. To avoid this situation, a repump laser that constantly excites the atoms from $F = 1$ into $F' = 2$ is needed. The repump transition helps to maintain non-zero population for $F = 2$ and keep the cooling process going on.

Two coils were built, each with sixty four turns of a $3mm \times 3mm$ cable with the coil diameter of ≈ 5 inch, for anti-Helmholtz configuration that produces quadrupole magnetic field as a part of MOT setup. The aim is to generate magnetic field gradient on the order of 10 Gauss/cm, which is the typical value for the trap. In order to compensate the background magnetic field for instance earth magnetic field, six bias coils were made. Each pair of these coils was to produce uniform magnetic field along each of the three orthogonal axes and therefore counter the background field.

The 1034nm laser was pointed into the chamber directly through a system of optics. In order to make a trap with decent potential depth, the initial beam waist must be as large as possible according to eq.(2.19). However, the largest beam waist that I managed to get was only 3mm due to the space constraint in optical setup. Upon going through the lens with a focal

length of 300mm mounted on the motorized translation stage, the final beam waist of the laser at the focus was calculated to be $\approx 33\mu$m. With the beam power of 6.2W, the trap depth was calculated to be $\approx 500\mu$K.

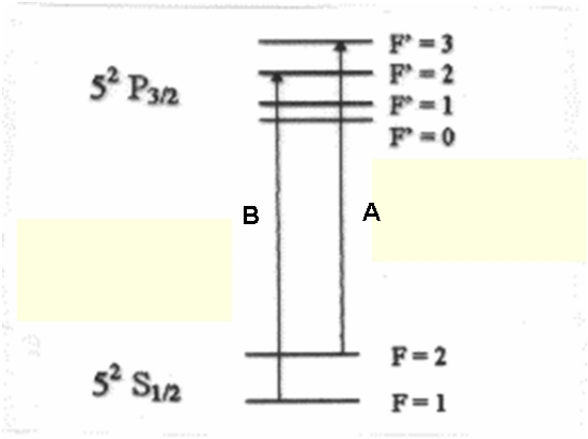

Figure 3.2: **Hyperfine Energy Level of Rubidium 87 For The Transition $S_{1/2} \rightarrow P_{3/2}$. A** and **B** correspond to the transition of cooling and repump interaction, respectively.

3.3 Translation

The transport of the trap from MOT chamber to the destination chamber was accomplished by translating a lens with 300mm focal length for 20cm. In order to maximize the retainability of the trap during the transport, a smooth and adiabatic motion is necessary. In my project, the transport

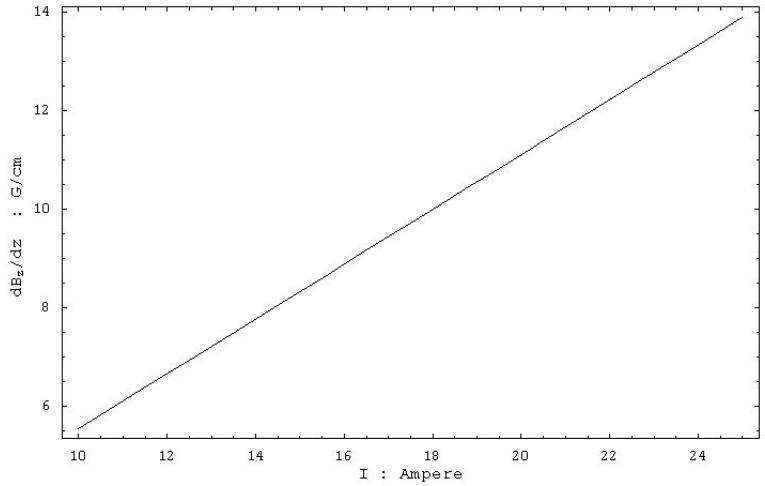

Figure 3.3: **Magnetic Field Gradient Against Applied Current.** This is the field gradient predicted at the centre of the MOT chamber for the coils separation of 7 inch. The field gradient exceeds 10G/cm as long as the applied current is above 18A.

of the laser-cooled atoms was achieved using a linear motorized translation stage (LX80L Linear Motor Table, Parker Automation) with the encoder resolution of 1μm, maximum travelling range of 750mm, maximum velocity of 3m/s, and maximum acceleration of 5G's. The motion of the translation stage depends on four input variables, namely velocity, acceleration , jerk (or $d\vec{a}/dt$), and travelling distance. For my application, I chose S-curve velocity profiles for both acceleration and deceleration, and without the motion with constant velocity in between. The reason was to maximize the duration for acceleration as well as deceleration and hence minimizing the heating due to short period jerk. The motion profiles are shown in Fig.(3.4) and Fig.(3.5).Since the chambers were 200mm apart, the computation for smooth motion was done based on this value. Possible heating might also arise due to the mechanical vibration of the stage. One of the solution to

this, as demonstrated by MIT group in 2001, is to isolate the vibration using rubber and lead weight [2]. However, my approach to this issue was different. This is because the proportional gain and the derivative gain of the translation stage can be adjusted such to optimize the mechanical power for the load as well as minimize the mechanical vibration of the stage. The motion of the translation stage can be observed through a build-in oscilloscope. This enabled trail-and-error approach in getting the optimum setting for both proportional gain and derivative gain of the translation stage. Fig.(3.6) shows the optimum motion profile as recorded by the build-in oscilloscope. The motion parameters were calculated for a range of time scales. The pattern of the motion profiles, however, remained the same such to maintain the smooth motion for all time scales.

Eq.(2.23) is only true for small z-displacement relative to the trap centre. If the displacement of an atom is too far off, the force that exerted by the trap may no longer enough to hold the atom from falling out during the transport. To know whether the trap has the ability to drive atoms at certain acceleration, we have to work out the maximum force that it can exert. Eq.(2.20) implies that $U \propto 1/w^2$, hence we have

$$U(r=0,z) \;=\; -\frac{U_0}{1+(z/z_R)^2}\,. \tag{3.20}$$

Differentiating eq.(3.20) and changing the sign, we have force equation as following

$$F(z) = \frac{U_0}{\left(1+(z/z_R)^2\right)^2}\frac{2z}{z_R^2} \tag{3.21}$$

$$= \frac{U_0}{z_R}\frac{2(z/z_R)}{\left(1+(z/z_R)^2\right)^2}\,. \tag{3.22}$$

Typically, maximum force is found at position $z = 0.5z_R$. Hence the expression for maximum force is given by

$$F_{max} = 0.64\frac{U_0}{z_R} = ma_{max}\,, \tag{3.23}$$

where m is the mass of an atom, in particular m=86.91u for Rb 87 [22], and a_{max} is the maximum acceleration that a trap can drive atoms. Substituting the required parameters into eq.(3.23), $a_{max} = 7.1ms^{-2}$. From the motion profile of the translation stage, the maximum acceleration of the trap is given by

$$a'_{max} = 1.6\frac{x_0}{T^2}\,, \tag{3.24}$$

where x_0 is the transport distance and T is the transport duration. In particular, for x_0=200mm, the minimum value of T such that $a'_{max} \leq a_{max}$ is 0.21s.

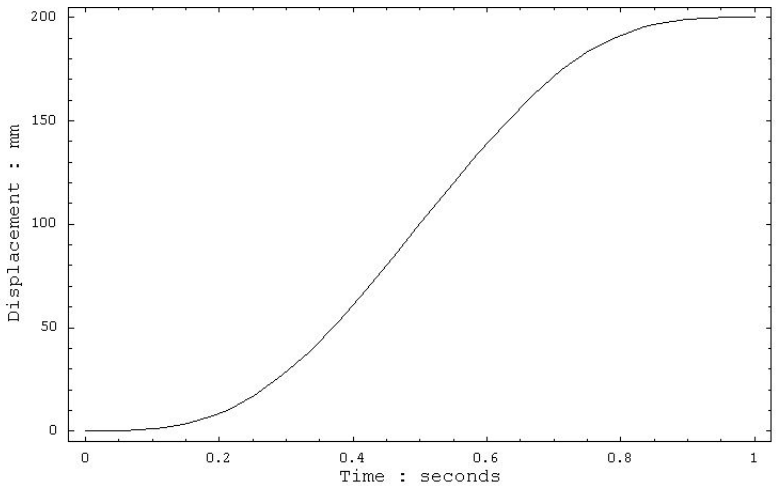

Figure 3.4: **Displacement of The Translation Stage Against Time (Transport Duration: 1 second).**

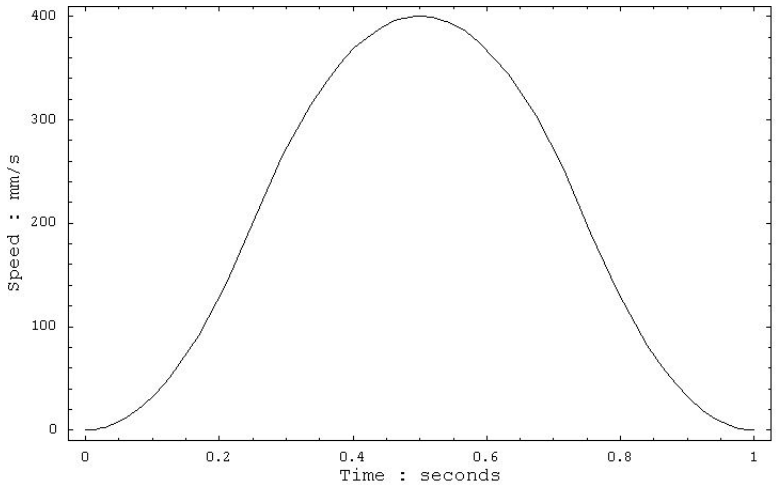

Figure 3.5: **Velocity of The Translation Stage Against Time (Transport Duration: 1 second).**

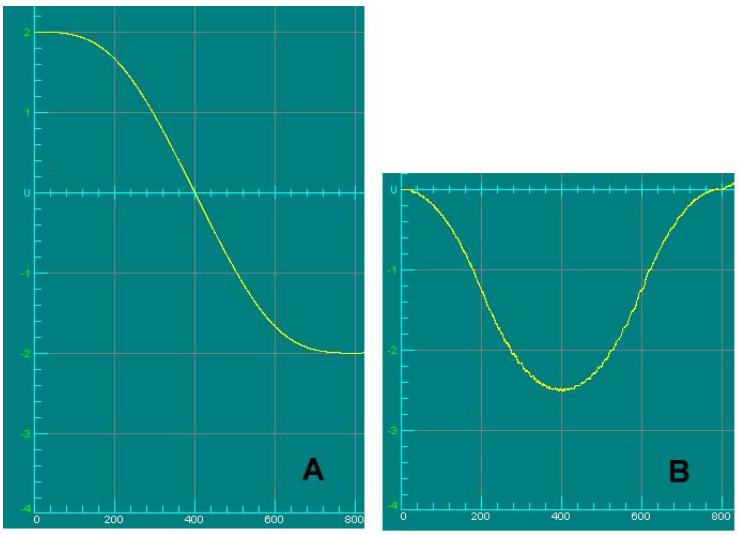

Figure 3.6: **Displacement And Velocity Profiles As Displayed By The Build-in Oscilloscope (Transport Duration: 0.8 second).** The profiles were taken for the motion in negative direction. **A**: x-axis: 0.2s/Div. y-axis: 50mm/Div. The profile shows a smooth curve which is similar to the computational result in Fig.(3.4). **B**: x-axis: 0.2s/Div. y-axis: 200mm/s/Div. The velocity profile shows a smooth curve with unobvious jag for optimum setting.

Chapter 4

Measurement

4.1 MOT Diagnostics

The measurement for the MOT population and temperature were done using a CCD camera looking into the MOT chamber through a window with 1.6cm in diameter. Before population measurement, quantum efficiency of the camera was determined by making use of a laser beam with known power. Quantum efficiency of a camera is defined as the number of photon that corresponds to a count in the camera pixel value. Measurement outcome showed that the quantum efficiency of the camera was $Q_E = 103.5 \pm 6.6$photon/count. The emission rate as measured by a camera with aperture diameter d at distance D away from the source is described by

$$Q_E \frac{dN_{photon}}{dt} = N_{atom} \left(\frac{d}{4D}\right)^2 \frac{\gamma}{2} \frac{I/I_s}{1 + I/I_s + (2\delta/\gamma)} \tag{4.1}$$

This equation assumes far field approximation where $\int_{\Delta\Omega} d\Omega = (d/4D)^2$ for

$D >> d$. Rearranging eq.(4.1), the trap population N_{atom} can be derived from the known parameters. The measurement was done and recorded as shown in Fig.(4.1). The maximum trap population was 96.6 ± 0.5 Million of atoms.

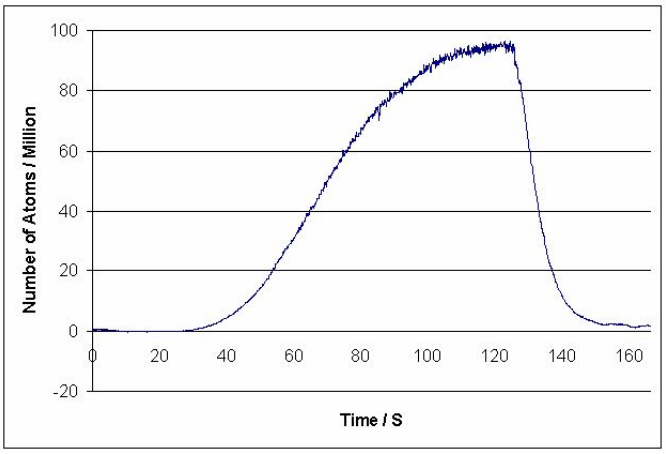

Figure 4.1: **The graph of Population against on-time of Rb Source.** After the source was turned off, the population of the trap decayed with the half-life of 5s.

Time-Of-Flight method was used in measuring the MOT temperature. It is a widely used technique where the trap is turned off to release the atoms into free ballistic flight. The resulting spatial distribution of the atoms cloud directly reflects the velocity distribution of the atoms at the time of release. The measurement was done in a sequence of steps. First the AOM swept the detuning from -20MHz to -200MHz for 3ms to optimize sub-Doppler cooling [23, 24]. The trap was then turned off for one or two milliseconds to let the atoms distributing themselves in Gaussian profile. The camera started to capture the MOT image immediately after the initial delay according to

the time steps of interests. The images captured at different time scales were fitted to Gaussian curves in order to derive the σ_{rms} (root mean squared radius) of the atoms cloud. σ_{rms} as a function of time is described by [25]

$$\sigma(t)^2 = \sigma_0^2 + \frac{k_B T}{M} t^2 \,. \tag{4.2}$$

For large time scale, σ_0^2 becomes insignificant and eq.(4.2) can be approximated as

$$\sigma(t) \approx t\sqrt{\frac{k_B T}{M}} \,, \tag{4.3}$$

where T and M are the temperature and the mass of the atom, respectively. Plotting the graph of $\sigma(t)$ against t, a linear curve is retrieved as shown in Fig.(4.2). Six sets of measurement data were collected and compared. Deriving from the gradient of the curves, temperature of the MOT was 15.4$\pm$ 2.3μK.

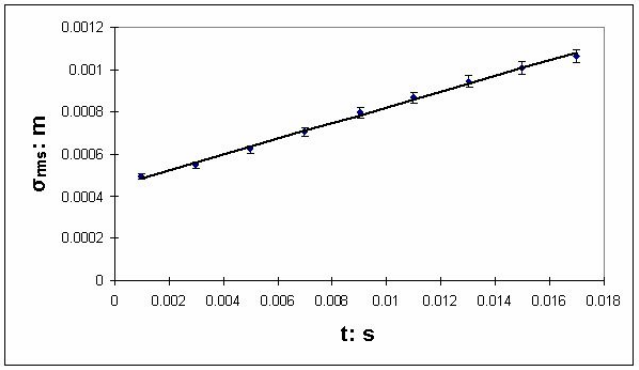

Figure 4.2: **The Graph of $\sigma(t)$ against t.**

4.2 Transport Efficiency

The dipole force trap was successfully loaded with atoms as shown in Fig.(4.3). The image of the trap was captured using a pixel camera (Princeton Instruments, Pixel 1024 7520-0001). The decay time of the population was investigated by capturing the image of the trap at different time scales after the MOT was dropped. A graph of the trap population was plotted as shown in Fig.(4.4). The initial population and the halflife of the trap were respectively ≈ 640 thousand of atoms and ≈ 0.44s. Then the trap was transported back and forth between the MOT and the destination chambers. The initial plan was to have the measurement done in the destination chamber, however, due to time constraint and the fact that the lab was moving to a new place, the plan changed. The measurement was done in the MOT chamber after the trap has been transported for a full trip with 40cm in travelling distance. The transport was then repeated for different time scales. Then the retainability for each time scale was calculated by taking into account of the trap loss due to decay. The retainability R is defined as

$$R = 100\% \times \frac{N'}{N} \,. \tag{4.4}$$

where N' and N are the population of the transported and the stationary trap at drop-time t, respectively. The data was tabulated and plotted as shown in Fig.(4.6). The experimental data collection was stopped for drop-time 1.5s onwards because the retainability was so close to 100% that it was indistinguishable between the transported and stationary trap due to significant background fluctuation.

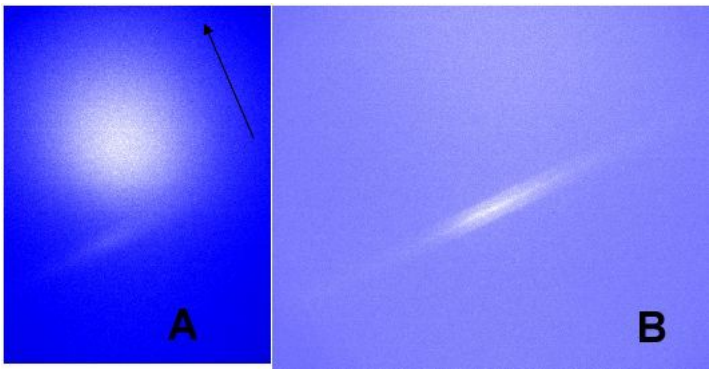

Figure 4.3: **Images of The Dipole Force Trap Captured at Different Drop Times. A:** The image captured after the MOT was dropped for 30ms. The arrow indicates the direction of drop. The spherical cloud in the picture is the MOT that was dropped and expended. **B:** The image of the dipole force trap can clearly be seen after 50ms of the drop time.

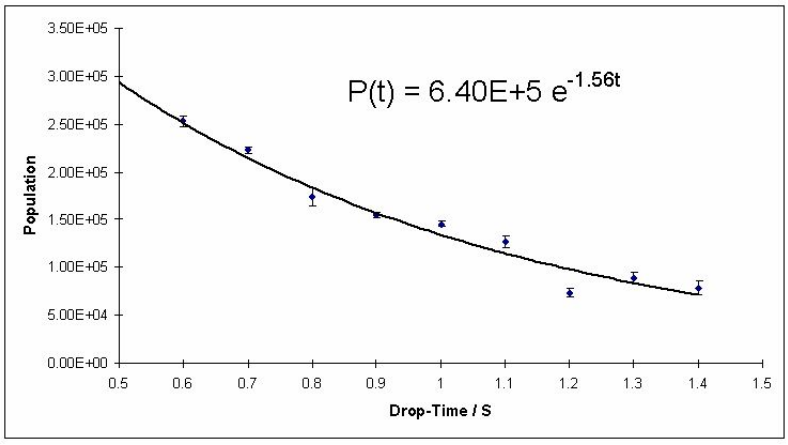

Figure 4.4: **Population of The Dipole Force Trap Against Drop-Time.** The error in measuring the population was mainly due to the background fluctuation. From the equation of the curve, the trap population was estimated to be around 640 thousand of atoms, with the half life of 0.44s.

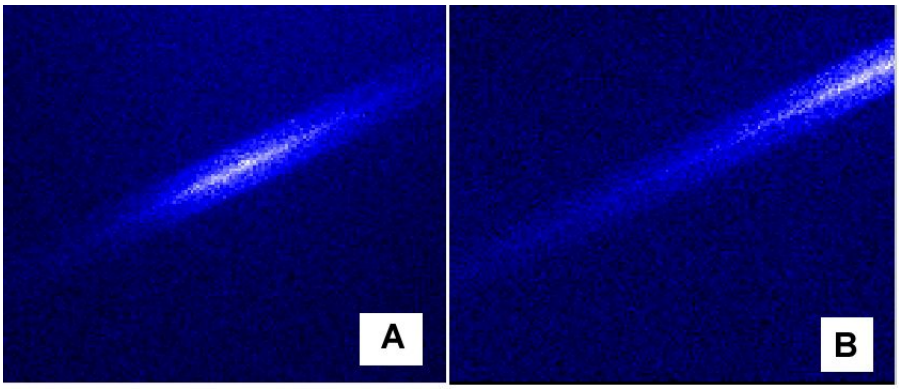

Figure 4.5: **Moving Dipole Force Trap. A:** The image of the trap captured at 50ms after the MOT was dropped. The motion was also triggered at the same moment. **B:** The same trap at 100ms, or 50ms after the motion was triggered. The trap was now on its way out to another chamber.

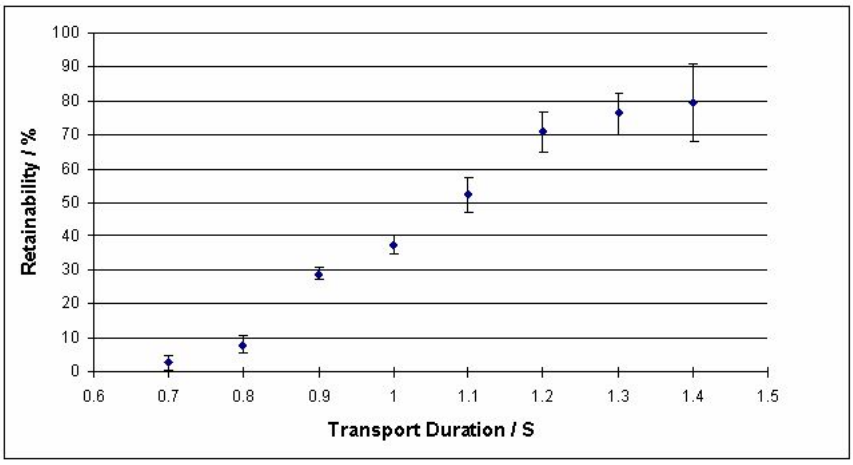

Figure 4.6: **Retainability Against Transport Duration (2 × 20 cm).** The retainability of the trap showed linear relation with the transport duration. The minimum duration for having non zero retainability was 0.7 seconds.

Chapter 5

Discussion and Conclusion

The imaging system for trap diagnostic was not operating at optimum level due to the constraint in accessible room around the MOT chamber. The camera was looking into the chamber through a window with 1.6cm in aperture diameter at 400mm away from the trap. The solid angle that covered by the camera was small. This posed a limitation in image resolution. Low resolution in trap image could potentially lead to several problems such as failure in BEC (Bose- Einstein Condensate) detection and uncertainty in measurement due to significant background fluctuation. As mentioned in previous chapter, the background fluctuation was a factor that stopped me from continuing my measurement for transporting the trap at longer time scales. One of the future works for this project is to construct an absorption imaging system that looks into the second chamber at a distance reasonably close to the trap. With such an imaging system, we can move on to study the heating due to the transport and examine the role of several parameters such as laser intensity and magnetic field strength in transport efficiency.

The laser power for the dipole force trap was 6.2W and the trap depth was calculated to be $\approx 500\mu$K. According to the section on translation, it was predicted that the minimum duration for the transport having non zero retainability should be 0.21s (one way, or 0.42s two way). However, experiment showed 0% retainability for transport duration that less than 0.35s (one way) referring to Fig.(4.6). The maximum driving force of the trap is proportional to $1/w^4$, therefore a small difference in beam waist may result in a huge difference in minimum transport duration. According to experimental outcome, the beam waist of the trap w is 37μm instead of the calculated value 33μm. This discrepancy could possibly due to imperfection in optics or laser mode. Hence the experimental value is still acceptable given that the discrepancy in minimum transport duration is only caused by a small difference in beam waist.

The MOT population can possibly be improved by finding the optimum magnetic field for the trap [26, 27]. By optimizing the population, loading of the dipole force trap could be more efficient as well. Currently the lifetime of the trap was only 0.44s. However, it is confident that the lifetime can be lengthened up to 10 seconds by optimizing the experimental parameters such as pressure of the UHV system. The transport efficiency can possibly be improved by having a vibration isolating system as suggested by a group from MIT in 2001 [2]. As one can see in Fig.(3.6), the motion was still having certain level of mechanical vibration throughout the transport. So it may be worthwhile to attempt in smoothening the velocity profile by

having additional weight and rubber. The MIT group also transported the trap with a trapezoidal acceleration profile [2] which is entirely different from the triangular acceleration profile that we used. Thus, the possible future work for this project may be to try out the transport with different motion profiles to optimize the transport efficiency.

Regardless of all the experimental issues, neutral atoms were successfully transported from one place to another for 40cm using a dipole force trap. Furture work for this experiment could be to transport a BEC using the same setup. The project can be further developed by exploring the idea of transporting BEC onto an atom chip.

Appendix A

Conductance of The Vacuum Components

A.1 Conductance of 4.5" Tee, C_1

To calculate the conductance, we need both the average thermal velocity of the gas v and the dimension of the Tee. At 22°C, v has the value of 464.5 ms^{-1}. The dimension of the Tee reads:

$$\begin{aligned} \text{inner diameter}, 2r &: 6.02\,\text{cm}\,, \\ \text{length (distance from one end to another)}, l &: 17.17\,\text{cm}\,, \\ \text{reduced length}, L = \frac{l}{r} &: 5.70\,. \end{aligned}$$

Substituting the readings and $v = 464.5\text{ms}^{-1}$ into eq.(3.8) and eq.(3.6), we have

$$a_1 = 0.285\,, \tag{A.1}$$

and

$$C' = 94.2\,l/s\,. \tag{A.2}$$

However, the effective conductance is approximately half of the calculated value because there is a right-angle bend in between the pump and the nipple reducer [28]. Therefore, the conductance of this section is

$$C_1 = \frac{C'}{2} = 47.1\,l/s\,. \tag{A.3}$$

A.2 Conductance of 4.5" × 2.75" Conical Nipple Reducer, C_2

The dimension of the conical nipple reducer reads:

$$\begin{aligned}
\text{maximum inner diameter}, 2r_{max} &: 6.02\,\text{cm}\,,\\
\text{minimum inner diameter}, 2r_{min} &: 3.48\,\text{cm}\,,\\
\text{length}, l &: 7.49\,\text{cm}\,,\\
\text{maximum reduced length}, L_{max} = \frac{l}{r_{max}} &: 2.49\,,\\
\text{minimum reduced length}, L_{min} = \frac{l}{r_{min}} &: 4.31\,.
\end{aligned}$$

The inner diameter of the conical nipple reducer varies from one end to another. To calculate the conductance, we need an entirely different approach which suits the tube with varying cross-sectional area along the hollow axis. One of the ways to get a rough approximation of the conductance is to treat the conical nipple reducer as two nipples in series connection, each with maximum diameter and minimum diameter respectively, and obtain the resultant conductance using the equation in combining conductance [16],

$$\frac{1}{C} = \sum_{j} \frac{1}{C_j} \,. \tag{A.4}$$

Using this method, the conductance reads $46.2\, l/s$. However, this value is just a rough estimation. Moreover, eq. (A.4) is only applicable to the case where the individual elements are separated by large volumes, such that the molecules exiting the prior conductance would have a place to completely randomize their distribution [16]. A more rigorous approach in calculating the conductance would be to make use of Haefer's method.

For my application, the cross-sectional area of the nipple reducer is increasing from one end to another so eq.(3.11) can be simplified as

$$\frac{1}{A_1}\left(\frac{1-a_{1\to n}}{a_{1\to n}}\right) = \sum_{1}^{n} \frac{1}{A_j}\left(\frac{1-a_j}{a_j}\right). \tag{A.5}$$

Converting eq.(A.5) from discrete sum into infinitesimal sum, whereby the conical nipple reducer is treated as if it is composed of $n \to \infty$ round tubes

$$\frac{1}{A_i}\left(\frac{1-a_2}{a_2}\right) = \int_0^L \frac{dl}{2\pi\left(\frac{l\,(r_f-r_i)}{L}+r_i\right)^3}\,, \tag{A.6}$$

where A_i is the cross-sectional area of the larger end, a_2 is the effective conductance of the conical nipple reducer, r_f and r_i are the respective radius of the large and the small ends, and L is the length of the conical nipple reducer along its hollow axis.

Integrating and rearranging eq.(A.6) to obtain the analytical expression for the transmission probability,

$$a_2 = \frac{4r_f^2}{4r_f^2 + L(r_i + r_f)}\,, \tag{A.7}$$

and substituting the resultant expression into eq.(3.6), we arrive at

$$C_2 = \frac{\pi v r_i^2 r_f^2}{4r_f^2 + L(r_i + r_f)}\,. \tag{A.8}$$

Substituting all the required parameters into eq.(A.7) and eq.(A.8), we have

$$a_2 = 0.505\,, \tag{A.9}$$

$$\text{and } C_2 = 55.7\,l/s\,. \tag{A.10}$$

The resultant conductance is $55.7\,l/s$, which is different from the estimated value $46.2\,l/s$ with a discrepancy of 17%.

A.3 Conductance of 2.02" × 2.02" × 2.02" Cube (Destination Chamber), C_3

For a vessel with rectangular cross-section, the transmission probability is given by [29]

$$a = c\,\frac{hb}{l(h+b)}\,, \tag{A.11}$$

where l, b, and h are the respective length, width, and thickness of the vessel, and c is a coefficient that varies with width-to-thickness ratio b/h. For cubes, b, h and l are the same. If $b/h = 1$, then coefficient c is also 1 [29]. Hence, from eq.(A.11), the transmission probability of a cube is

$$a_3 = \frac{1}{2}\,. \tag{A.12}$$

However, the inlet and the outlet are perpendicular to each other so another factor of 1/2 is introduced [28]. Altogether, the conductance of the cube is

$$C_3 = \left(\frac{1}{2}\right)\left(\frac{1}{2}\right)\frac{v}{4}A = 77.0\,l/s \tag{A.13}$$

A.4 Conductance of 1.33" Nipple, C_4

The nipple has the dimension as follows

$$\begin{aligned} \text{inner diameter}, 2r &: 1.73\,\text{cm}\,, \\ \text{length}, l &: 7.62\,\text{cm}\,, \\ \text{reduced length}, L = \frac{l}{r} &: 8.82\,. \end{aligned}$$

Substituting the parameters into eq.(3.8) and eq. (3.6), the transmission probability and the conductance of the nipple are respectively

$$a_4 = 0.210\,, \tag{A.14}$$

$$\text{and } C_4 = 5.71\,l/s\,. \tag{A.15}$$

Appendix B

Raw Data

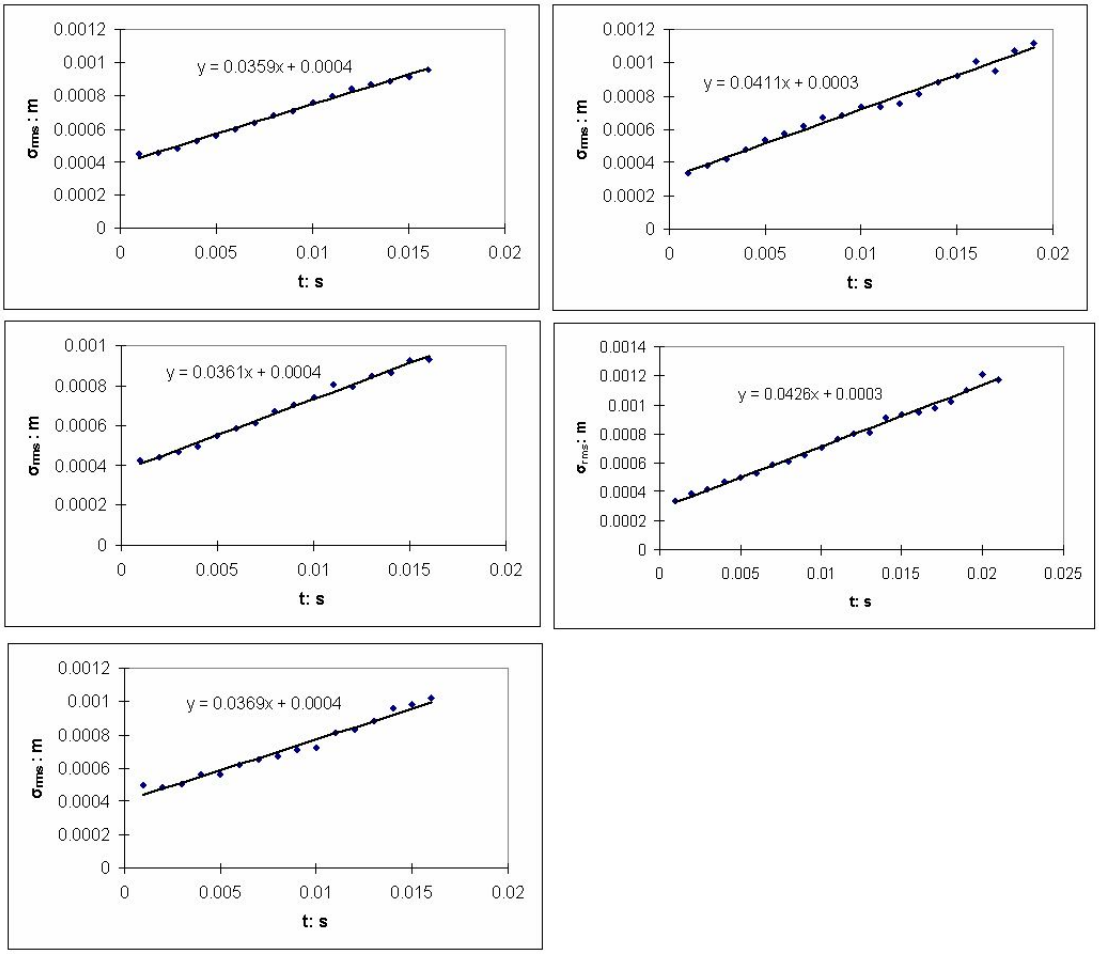

Figure B.1: **MOT Temperature Measurement - $\sigma(t)$ against t.**

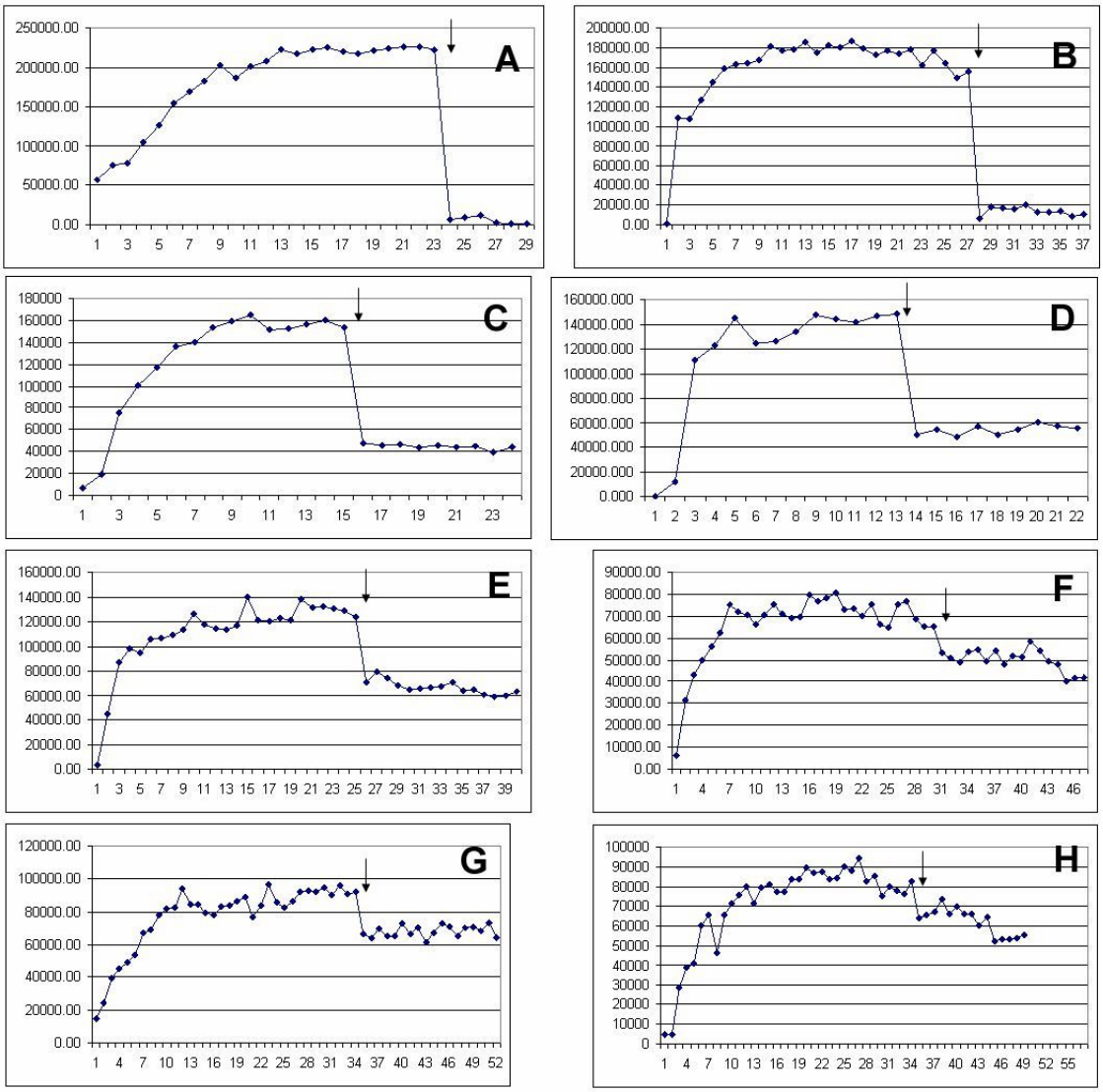

Figure B.2: **Dipole Force Trap Population Measurement - Trap Population against Time/s.** Arrows indicate the shift in measurement from stationary traps to transported traps. Transport duration: **A:** 0.7s. **B:** 0.8s. **C:** 0.9s. **D:** 1.0s. **E:** 1.1s. **F:** 1.2s. **G:** 1.3s. **H:** 1.4s.

Appendix C

Experimental Setup

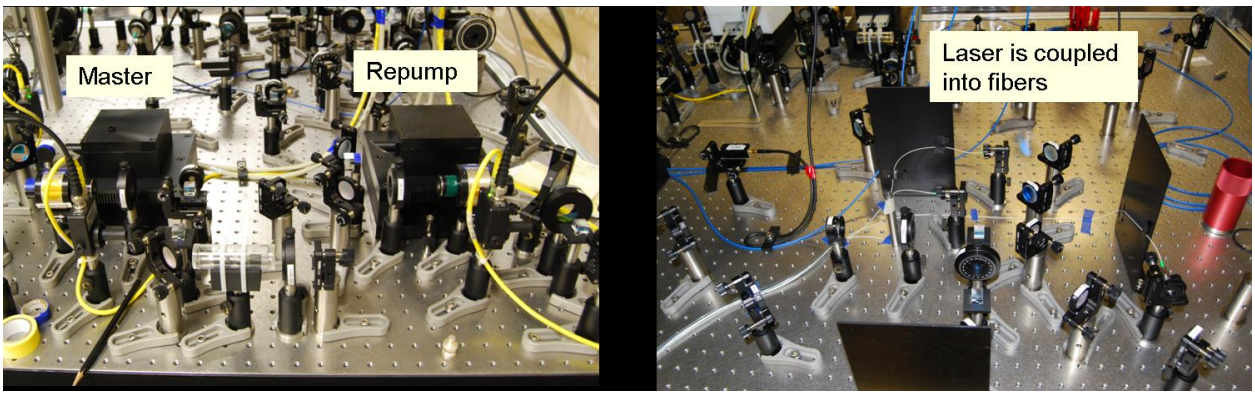

Figure C.1: **780nm Laser.**

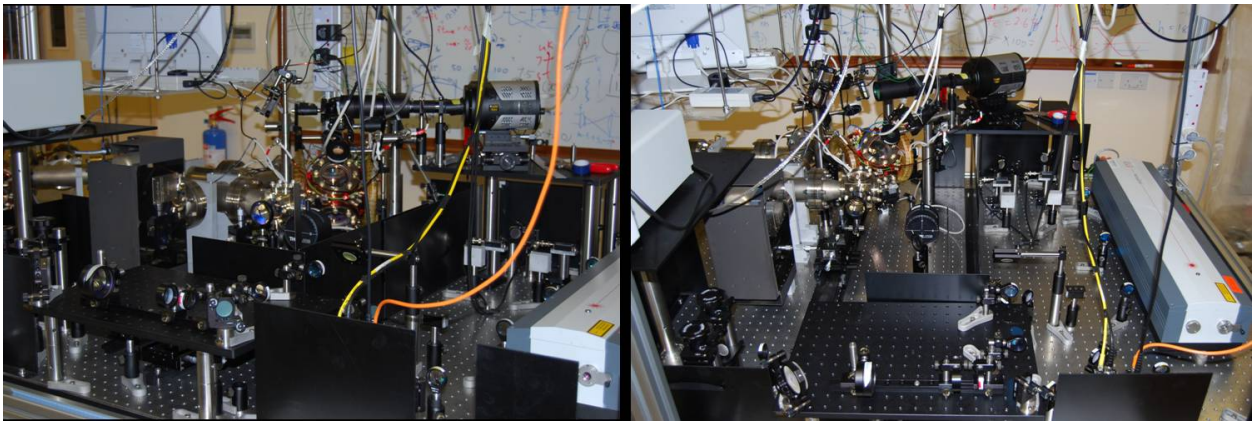

Figure C.2: **Setup Overview.**

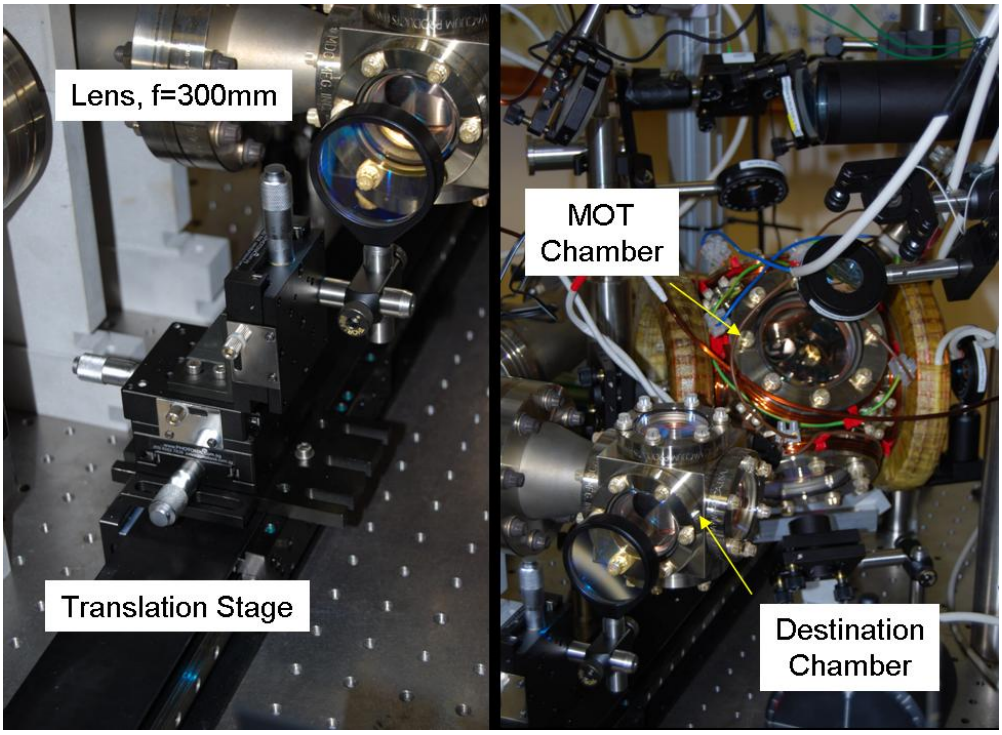

Figure C.3: **Translation Stage and Chambers.**

Bibliography

[1] M. Greiner, I. Bloch, T. W. Hansch, and T. Esslinger, Phys. Rev. A **63**, 031401 (2001).

[2] T. L. Gustavson, A. P. Chikkatur, A. E. Leanhardt, A. Grlitz, S. Gupta, D. E. Pritchard, and W. Ketterle, Phys. Rev. Lett. **88**, 020401 (2001).

[3] L. Pruvost, D. Marescaux, O. Houde, and H. T. Duong, Opt. Commun. **166**, 199-209 (1999).

[4] K. Szymaniec, H. J. Davies, and C. S. Adams, Europhys. Lett. **45**, 450-455 (1999).

[5] H. J. Davies, K. Szymaniec, and C. S. Adams, J. Phys. B: At. Mol. Opt. Phys. **33**, 4079-4086 (2000).

[6] M. J. Renn, D. Montgomery, O. Vdovin, D. Z. Anderson, C. E. Wieman, and E. A. Cornell, Phys. Rev. Lett. **75**, 3253 - 3256 (1995).

[7] M. J. Renn, E. A. Donley, E. A. Cornell, C. E. Wieman, and D. Z. Anderson, Phys. Rev. A **53**, R648 - R651 (1996).

[8] S. Chu, L. Hollberg, J. E. Bjorkholm, A. Cable, and A. Ashkin, Phys. Rev. Lett. **55**, 48 (1985).

[9] J. Prodan, A. Migdall, W. D. Phillips, I. So, H. Metcalf, and J. Dalibard, Phys. Rev. Lett. **54**, 992 (1985).

[10] J. F. Christopher, *Atomic Physics*, Oxford University Press (2005).

[11] E. L. Raab, M. Prentiss, A. Cable, S. Chu, and D. E. Pritchard, Phys. Rev. Lett. **59**, 2631 - 2634 (1987).

[12] H. J. Metcalf and v. d. Straten, *Laser Cooling and Trapping*, Springer (1999).

[13] G. A. Askar'yan, Zh. Eksp. Teor. Fiz. **42**, 1360 (1962); [Sov. Phys. JETP **15**, 943 (1962)].

[14] J. P. Gordon and A. Ashkin, Phys. Rev. A **21**, 1606 - 1617 (1980).

[15] R. Grimm, M. Weidemller, and Y. B. Ovchinnikov, Adv. At. Mol. Opt. Phys., **42**, 95 (2000).

[16] John F.O'Hanlon, *A user guide to vacuum technology 3rd edition* (Wiley, 2003).

[17] A. S. Berman, J. Appl. Phys. **36**, 3356 (1965).

[18] T. W. Hnsch, I. S. Shahin, and A. L. Schawlow, Phys. Rev. Lett. **27**, 707 - 710 (1971).

[19] V. S. Letokhov, *Laser Control of Atoms And Molecules*, Oxford University Press (2007).

[20] H. L. Stover and W. H. Steier, Appl. Phys. Lett. **8**, 91 (1966).

[21] C. L. Tang and H. Statz, J. Appl. Phys. **38**, 323 (1967).

[22] D. A. Steck. http://steck.us/alkalidata.

[23] M. Drewsen, Ph. Laurent, A. Nadir, G. Santarelli, A. Clairon, Y. Castin, D. Grison, and C. Salomon, Appl. Phys. B **59**, 283 (1994).

[24] C. G. Townsend, N. H. Edwards, C. J. Cooper, K. P. Zetie, C. J. Foot, A. M. Steane, P. Szriftgiser, H. Perrin, and J. Dalibard, Phys. Rev. A 52, 1423 - 1440 (1995).

[25] T. M. Brzozowski, M. Maczynska, M. Zawada, J. Zachorowski, and W. Gawlik, J. Opt. B: Quantum Semiclass. Opt. **4**, 62-66 (2002).

[26] W. Petrich, M. H. Anderson, J. R. Ensher, and E. A. Cornell, J. Opt. Soc. Am. B **11**, 1332 (1994).

[27] J. Dalibard and C. Cohen-Tannoudji, J. Opt. Soc. Am. B **6**, 2023 (1989).

[28] D. H. Davis, J. Appl. Phys. **31**, 1169 (1960).

[29] G. L. Saksaganskii, *Molecular flow in complex vacuum systems* (Gordon and Breach Science Publishers, 1988).